Warp or lag? The ionized and neutral hydrogen gas in the edge-on dwarf galaxy UGC 1281

Kamphuis, Peter; Peletier, R. F.; van der Kruit, P. C.; Heald, G. H.

Published in:
Monthly Notices of the Royal Astronomical Society

DOI:
10.1111/j.1365-2966.2011.18641.x

Monthly Notices of the ROYAL ASTRONOMICAL SOCIETY

Mon. Not. R. Astron. Soc. **414,** 3444–3457 (2011) doi:10.1111/j.1365-2966.2011.18641.x

Warp or lag? The ionized and neutral hydrogen gas in the edge-on dwarf galaxy UGC 1281

P. Kamphuis,[1,2★†] R. F. Peletier,[1] P. C. van der Kruit[1] and G. H. Heald[3]

[1]*Kapteyn Astronomical Institute, University of Groningen, Postbus 800, 9700 AV, Groningen, the Netherlands*
[2]*Astronomisches Institut der Ruhr-Universität Bochum, Universitätsstr. 150, 44780 Bochum, Germany*
[3]*Netherlands Institute for Radio Astronomy (ASTRON), 7990 AA Dwingeloo, the Netherlands*

Accepted 2011 March 4. Received 2011 March 4; in original form 2010 July 4

ABSTRACT

The properties of gas in the haloes of galaxies constrain global models of the interstellar medium. Kinematical information is of particular interest since it is a clue to the origin of the gas. Until now mostly massive galaxies have been investigated for their halo properties.

Here we report on deep H I and Hα observations of the edge-on dwarf galaxy UGC 1281 in order to determine the existence of extraplanar gas and the kinematics of this galaxy. This is the first time a dwarf galaxy is investigated for its gaseous halo characteristics. We have obtained Hα integral field spectroscopy using PPAK at Calar Alto and deep H I observations with the Westerbork Synthesis Radio Telescope (WSRT) of this edge-on dwarf galaxy. These observations are compared to 3D models in order to determine the distribution of H I in the galaxy.

We find that UGC 1281 has Hα emission up to 25 arcsec (655 pc) in projection above the plane and in general a low Hα flux. Compared to other dwarf galaxies UGC 1281 is a normal dwarf galaxy with a slowly rising rotation curve that flattens off at 60 km s^{-1} and a central depression in its H I distribution. Its H I extends 70 arcsec (1.8 kpc) in projection from the plane. This gas can be explained by either a warp partially in the line-of-sight or a purely edge-on warp with rotational velocities that decline with a vertical gradient of 10.6 ± 3.7 km s^{-1} kpc^{-1}. The line-of-sight warp model is the preferred model as it is conceptually simpler. In either model the warp starts well within the optical radius.

Key words: galaxies: dwarf – galaxies: haloes – galaxies: ISM – galaxies: kinematics and dynamics – galaxies: spiral – galaxies: structure – UGC 1281.

1 INTRODUCTION

The discovery of a very extended H I halo in NGC 891 has shown that 21-cm observations are a powerful tool to study the structure and kinematics of gaseous haloes. Since this discovery (Swaters, Sancisi & van der Hulst 1997) many investigations have followed studying this (Oosterloo, Fraternali & Sancisi 2007) and other galaxies. Investigations at 21 cm, as well as other wavelengths, have shown that NGC 891 is not a special case in having a gaseous halo (Schaap, Sancisi & Swaters 2000; Lee et al. 2001; Rossa & Dettmar 2003; Barbieri et al. 2005; Westmeier, Braun & Thilker 2005; Boomsma et al. 2008).

It is thought that a large part of this halo gas is brought up from the disc by galactic fountains (Shapiro & Field 1976; Bregman 1980). In this model supernovae explosions expel the hot hydrogen gas from the disc into the halo. In the halo the gas cools down and condenses before returning to the disc. Studies of massive galaxies have shown that this mechanism is very likely at work in several galaxies, either inferred from the fact that the extraplanar H I is concentrated towards the disc (Oosterloo et al. 2007) or that the majority of high-velocity clouds are located near the bright inner disc (Boomsma et al. 2008).

The gas in the halo of NGC 891 shows rotational velocities that are lower than the velocities of the gas in the disc. This 'lag' is observed in H I (Fraternali et al. 2005) as well as in Hα (Heald et al. 2006; Kamphuis et al. 2007) and determined to be linear with a magnitude of $\sim$16 km s^{-1} kpc^{-1} in the vertical direction.

Simulations have shown that the lag cannot be explained by galactic fountains alone (Fraternali & Binney 2008). Together with other observational facts, such as the low metallicity of the high-velocity clouds (HVCs) and the presence of filaments and other irregular gaseous structures in the halo (Sancisi et al. 2008), this has given rise to the idea that the halo must also be partially formed from gas that has been accreted from the intergalactic medium (IGM)

★Humboldt Research Fellow.
†E-mail: peter.kamphuis@astro.rub.de

or companion galaxies. However, the gradients by themselves do not necessarily require accretion from the IGM (Benjamin 2002; Barnabè et al. 2006).

Even though this lagging behaviour is observed in other galaxies than NGC 891 – e.g. Heald et al. (2007) studied two other large galaxies and found a lag in both of them – it is not known whether it occurs in all gaseous haloes. Until now, kinematical studies have focused on massive galaxies and one low surface brightness (LSB) galaxy (Matthews & Wood 2003) but dwarf galaxies have not yet been investigated for a kinematic lag.

Here we present deep H I and Hα observations of the edge-on dwarf galaxy UGC 1281 and analyse the kinematics of the H I and Hα in and above the plane. The 21-cm line emission was observed with the Westerbork Synthesis Radio Telescope (WSRT) and the Hα with the Integral Field Unit (IFU) PPAK on the 3.5-m telescope at Calar Alto.

The edge-on orientation of UGC 1281 provides us with an excellent opportunity to study the vertical structure of gas in a dwarf galaxy. Our H I observations of UGC 1281 are some of the deepest observations ever conducted on a dwarf galaxy, and never before has an edge-on dwarf galaxy been observed to this depth.

UGC 1281 is a nearby edge-on dwarf galaxy [$M_B = -15.8$, Swaters & Balcells (2002)] with a systemic velocity of 156 km s^{-1} at a distance of 5.4 Mpc (Karachentsev et al. 2004). The galaxy has an angular diameter of 4.46 arcmin (D_{25}) (de Vaucouleurs et al. 1992) on the sky which would translate to 7 kpc at the given distance. van Zee (2000, 2001) measured the star formation rate in UGC 1281 to be very low (0.0084 M$_\odot$ yr^{-1}). However, this should be considered as a lower limit since the Hα flux was not corrected for internal extinction. These observations are supported by the non-detections in radio continuum (Hummel, Beck & Dettmar 1991) and *IRAS*. Indeed, Rossa & Dettmar (2003) observed UGC 1281 as a part of their extraplanar diffuse ionized gas (DIG) survey and could not detect any extraplanar Hα in this dwarf galaxy. All these observations indicate a very low star formation rate in UGC 1281.

Under the assumption that gaseous haloes are created by processes related to star formation, little to no halo is expected when the star formation rate (SFR) is low. However, in a dwarf galaxy gas might easily escape from the disc due to the weak potential. Also, even though small galaxies are not expected to accrete baryonic matter at lower redshifts (Hoeft & Gottloeber 2010), UGC 1281 is in the transition region, between accreting and non-accreting galaxies, and therefore a modest amount of lagging extraplanar gas might be present if the vertical gradient is predominantly formed by the accretion of matter.

This article is structured as follows. In Section 2 we will describe the observations and data reduction. Section 3 will contain the results of the observations followed by a presentation of our models in Section 4. We will discuss our results in Section 5 and summarize in Section 6.

2 OBSERVATIONS AND DATA REDUCTION

2.1 Radio data

The 21-cm line emission, or H I, observations were obtained with the WSRT during four nights in 2004 September. In total four complete 12-h observations were performed using the Maxi-Short configuration. This configuration gives the optimum performance for imaging extended sources. This is because it provides a good sampling of the inner $U - V$ plane with the shortest baseline of 36 m. The longest baseline is 2754 m. An overview of the observational parameters is given in Table 1.

Table 1. Log of the H I observations.

Parameter	Value
Observation date	2004 September
Total length of observation (h)	4 × 12
Velocity centre of band (km s^{-1})	156
Total bandwidth (MHz)	10
Channels in obs.	1024
Channel sep. in obs. (kHz)	9.77
Channels in final cube	61
Vel. res. after Hanning smoothing (km s^{-1})	8.24

The data were reduced using the MIRIAD package (Sault, Teuben & Wright 1995). Care was taken not to include data affected by solar or other interferences. Before and after each 12-h observation a calibration source (3C147 and CTD93) was observed, thus enabling us to determine the spectral response of the telescope. During each 12-h observation no additional (phase) calibration sources were observed, as is the standard practice with the WSRT. Due to the large bandwidth, the time variations can be determined from the self-calibration of the detected sources in the continuum image constructed from the channels free of line emission. In this case UGC 1281 itself was not detected in continuum emission.

After the reduction and calibration, additional analysis was performed with the GIPSY package (van der Hulst et al. 1992). The final cube was reduced to 61 velocity channels with a velocity spacing of 4.12 km s^{-1}, which results in a velocity resolution after Hanning smoothing of 8.24 km s^{-1}. The original cube has a spatial resolution of 25.0 × 13.4 arcsec^2. This cube was smoothed to two cubes with circular beams of 26 arcsec (0.68 kpc) and 60 arcsec (1.57 kpc) to avoid beam orientation effects and to detect low-level emission (see Table 2).

For the calculation of the minimum detectable column in Table 2, we used a velocity width of 16.5 km s^{-1}, because real emission will never appear in a single channel.

The position of the centre of the galaxy, as determined by Swaters & Balcells (2002) from *R*-band photometry, was set to zero in the three cubes and they were rotated by 50° [position angle (PA) = 40°, Swaters & Balcells (2002)] to orient the major axis of the galaxy parallel to the *x*-axis of the image.

2.2 IFU data

The Hα was observed with the PPAK integral field unit on the 3.5-m telescope at Calar Alto (Kelz et al. 2006). Three positions were observed in one night (see Table 3). At each position several exposures were taken. Two positions were observed for 3 × 1200 s (north and centre) and one for 3 × 600 s (south). The lower exposure time of the southern field was due to twilight. The pointings of the north and south fields were shifted by ∼± 76 arcsec, compared to the centre, along an axis with a PA slightly offset (∼10° offset) from the PA of the galaxy. This was done to ensure a good coverage of extraplanar Hα. The spectra cover a wavelength range of ∼5500–7000 Å with a resolution of 4.1 Å (187 km s^{-1} at Hα). The conditions were partially photometric with a mean seeing of 1.3 arcsec, which is much less than the fibre size (2.7 arcsec).

For the reduction of the PPAK spectra the IRAF package was used. The steps in the DOHYDRA Guide (Valdes 1995) were followed manually to ensure complete control over the reduction. The only

Table 2. Parameters of the H I data cubes.

Parameter	Full resolution	Circular beam	Low resolution
Spatial resolution (arcsec)	25.0 × 13.4	26.0 × 26.0	60.0 × 60.0
Beam size (kpc)	0.65 × 0.35	0.68 × 0.68	1.57 × 1.57
rms noise per channel (mJy beam^{-1})	0.44	0.50	0.72
Minimum detectable column density (3σ; cm^{-2})	7.1 × 10^{19}	4.0 × 10^{19}	1.1 × 10^{19}

Table 3. Log of the Hα observations.

Parameter	Field 1 and 2	Field 3
Name	North and centre	South
Observation date	2006 September	Same
Exposure time (s)	3600	1800
Central wavelength (Å)	6273	6273
Total bandwidth (Å)	1628	1628
Channels in obs.	1050	1050
Channel sep. in obs. (Å)	1.55	1.55
Channel separation (km s^{-1}) at Hα	70.8	70.8

deviation taken from the steps as described in this guide was that we traced the apertures on the science frames themselves. This was done because there was more than enough continuum emission in each spectrum and there was no need to introduce additional errors due to shifting of the apertures.

For the initial wavelength calibration seven lines of an HeNe+ThAr lamp were used. Afterwards a fine-tuning calibration was performed with five sky lines in each science frame. For the sky-line subtraction a total of 95 sky fibres from the three pointings were used. All the sky fibres were checked for inconsistencies and, except for sky fibres with the galaxy in their field of view, none was found.

After the reduction and wavelength calibration, the different exposures of each field were combined by calculating the median of the separate exposures. No clipping was applied. The three fields were then positioned into one field by overlaying the continuum images of the fields on top of an *R*-band DSS image. By taking special care that the five stars in the three fields were aligned properly, this procedure resulted in a position error less than 1 arcsec, which is smaller than the 2.7-arcsec fibre size.

Our reduced and calibrated data were further analysed with a combination of IDL programs produced by the SAURON collaboration (e.g. de Zeeuw et al. 2002) and ourselves. The data were Voronoi binned with the VORONOI_2D_BINNING IDL program (Cappellari & Copin 2003) to obtain a higher S/N ratio (S/N > 20). Like the H I, the central position of the galaxy was set to (0,0) and the galaxy was rotated by 50° to align the major axis with the *x*-axis.

3 RESULTS

Here, we first discuss the distribution and kinematics of the hydrogen that can be directly derived from the data. In Section 5 we will compare the distributions and kinematics of the ionized and neutral gas, highlight the differences and similarities and discuss possible interpretations of these distributions.

3.1 Gas distribution

3.1.1 Hα distribution

Fig. 1 shows the Hα flux obtained with the PPAK IFU instrument. The flux in each bin was determined by fitting a Gaussian, with the IDL routine GAUSSFIT, to an average of the spectra in each bin. The area under this Gaussian is then considered to be the flux in each bin. All the fitted Gaussians were inspected by eye, and none of the fitted lines showed significant deviations from Gaussian. For display purposes the log values of the flux are displayed. For the same reason the bins without emission are simply taken away from the data and thus not displayed. Overlaid on the image are the contours of an integrated H I (zeroth moment) map.

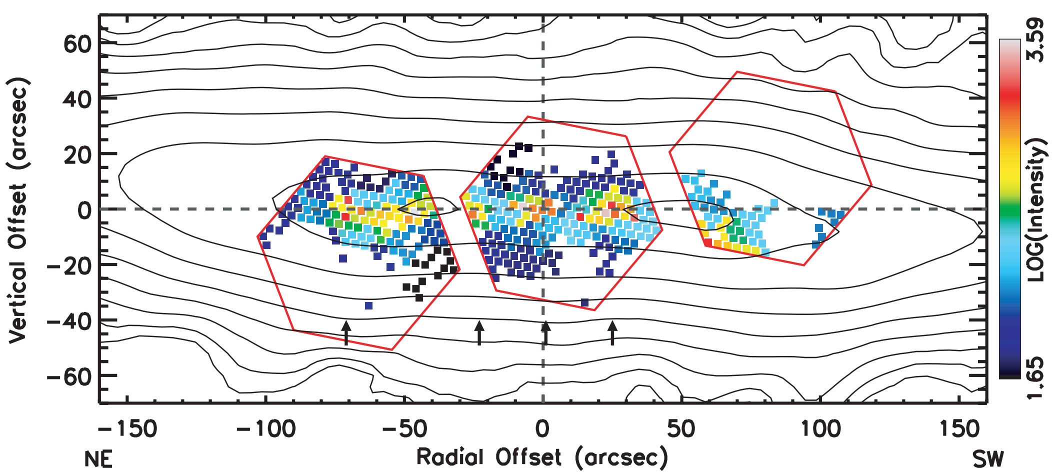

Figure 1. Integrated Hα flux map of UGC 1281. The map was constructed by taking the log of the area under the fitted Gaussian in each spectrum. The red lines indicate the full field of view of the PPAK observations. Overlaid in black are the contours of an integrated H I (zeroth moment) map. The contours are at the 1.5σ, 3σ, 6σ, 12σ, 24σ, 48σ, 96σ, 192σ and 273σ levels of the data where σ = 2.2 mJy beam^{-1}. The arrows indicate the positions of the velocity cuts parallel to the minor axis in Fig. 6.

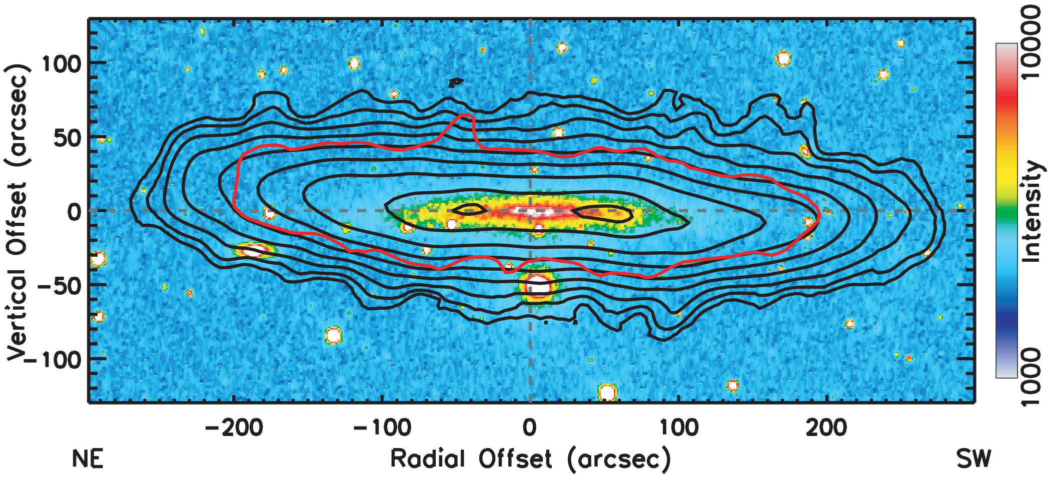

Figure 2. Continuum image in the red from the DSS 2 overlaid with contours of our integrated H I flux map of UGC 1281 (see text). The black contours are the same as in Fig. 1. The red contour indicates the 3σ contour of the WHISP observations.

The first thing we see from Fig. 1 is that the ionized hydrogen is mostly located in five or six distinct peaks but that there is low-level emission almost everywhere in the central field of view. The distinct peaks can most likely be associated with large H II regions in the galaxy whereas the low-level emission is indicating a diffuse ionized component. The two innermost peaks at the north-east (NE) and south-west (SW) sides of the centre of the galaxy might be caused by a ring-like structure or central depression in the distribution. This seems to be implied by their equal distance from the centre; however, they could also be normal H II regions.

A warp is clearly seen in the H II regions as well as the diffuse emission. The peak of the emission starts to deviate from the major axis at a radial distance of ∼50 arcsec (1.3 kpc). In the SW of the galaxy we see an exception to this behaviour with a large ionized hydrogen peak below the major axis, where the diffuse emission still seems to be mostly on the major axis. This seems to indicate an H II region that is either somewhat offset from the plane or located on the outskirts of the galaxy. If the warp is partially along the line of sight, the outer parts will not only experience a change in position angle but also in inclination. Thus if this H II region is located on the outskirts of the galaxy, its position can be in the (warped) plane of the galaxy.

The Hα distribution could, in theory, be severely affected by internal dust extinction, especially in the edge-on orientation. However, in the case of UGC 1281 this seems unlikely because no clear dust lane can be observed in the *HST* imaging of UGC 1281 (Bomans & Weis 2008) and dwarf galaxies are expected to have a low metallicity (Pilyugin, Contini & Vílchez 2004) and therefore little dust content. The reddish colour of UGC 1281 (Makarova & Karachentsev 1998) is most likely caused by the absence of a large young stellar population. This once more confirms the idea that UGC 1281 has a low SFR.

In our data the maximum distance to the mid-plane where diffuse gas is still detected is ∼25 arcsec (0.65 kpc). This is similar to the extent of the stars [$\frac{1}{2}d_{25,\rm minor}$ = 18 arcsec, van Zee (2000); $\frac{1}{2}d_{25,\rm minor}$ = 23 arcsec, de Vaucouleurs et al. (1992)]. If we fit an exponential to the inner vertical intensity profile of the ionized gas we find a scaleheight of 8.5 arcsec (0.22 ± 0.03 kpc) assuming that the galaxy is seen perfectly edge-on. When we follow the same procedure for the continuum emission in our spectra and an *I*-band image[1] we find a scaleheight of 7.6 arcsec (0.20 ± 0.01 kpc) and 8.0 arcsec (0.21 ± 0.01 kpc), respectively.

3.1.2 H I distribution

Fig. 2 shows the DSS 2 red image of UGC 1281 overlaid with the contours of our integrated H I flux map. This H I map was constructed by adding all the channels of the Circular Beam data cube. To keep the addition of noise to a minimum, only regions that are above 3σ in the low-resolution cube (see Table 2) were considered.

From Fig. 2 we can see that the H I of UGC 1281 is at first glance quite symmetrically and evenly distributed. However, a closer look reveals asymmetries and peculiarities in the H I distribution. It warps away from the major axis at about 90 arcsec (2.4 kpc) on the south-west and at about 100 arcsec (2.6 kpc) on the north-east. The warp initially shows the normal S-shape observed in many edge-on galaxies (García-Ruiz, Sancisi & Kuijken 2002) but bends back to the plane of the inner disc at larger radii. This behaviour is seen especially at the south-west side, at a radial offset of ∼200 arcsec. This warp was already observed by García-Ruiz et al. (2002) in the WHISP observations of this galaxy (van der Hulst, van Albada & Sancisi 2001).

When we compare the lowest contour in the integrated moment map of the WHISP observations with our own (see Fig. 2, red contour), we see that in our observations more emission is detected in the radial as well as in the vertical direction. The growth in both directions is similar in extent and this indicates that even with our deep observations we might not be detecting the lowest levels of emission of this galaxy.

Furthermore, the H I distribution displays a central depression. This depression appears as a ring around the centre of the galaxy and ranges from 10 to 40 arcsec (0.26–1.05 kpc) radial offset from the centre of the galaxy. It appears to be symmetrical around the centre of the galaxy.

[1] Obtained through the NASA extragalactic data base.

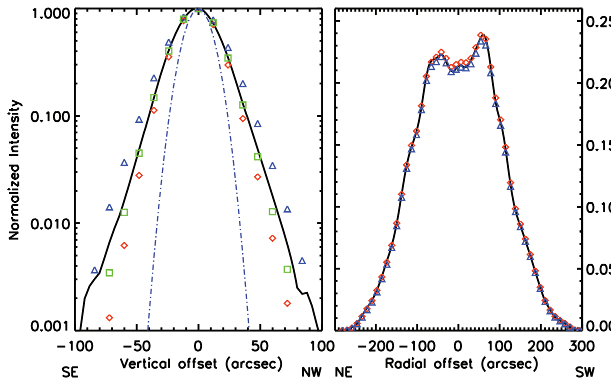

Figure 3. Intensity profiles of the observed H I. Left-hand figure: vertical intensity profile, averaged over the inner 100 arcsec in the radial direction and normalized to the peak intensity. Right-hand figure: radial intensity profile, averaged over the inner 40 arcsec of the galaxy in the vertical direction. Black line: data, Green squares: best-fitting model, Red diamonds (blue triangles): best-fitting model with a scaleheight −2 arcsec (+4 arcsec) (see Section 4). Blue dotted–dashed line: beam.

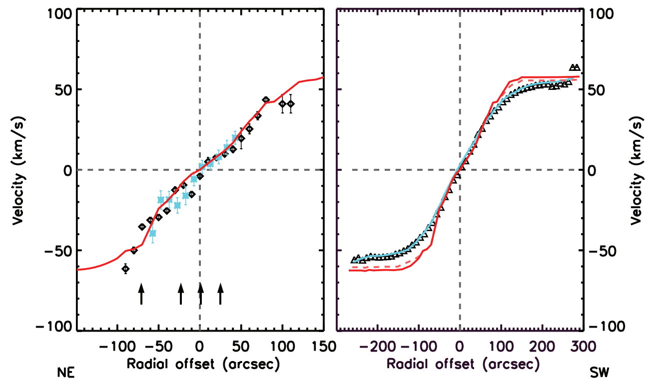

Figure 5. Velocities along the major axis. The left-hand panel shows the Hα velocities: black symbols are the PPAK data presented in this paper, blue symbols are the data obtained by Kuzio de Naray et al. (2006). The right-hand figure shows H I velocities: black symbols are the H I, the blue line shows the velocities obtained from the model. The red lines are the input unprojected rotation curves of the best-fitting models described in Section 4. The arrows indicate the positions of the velocity cuts parallel to the minor axis in Fig. 6.

The H I in UGC 1281 shows significant extensions away from the major axis. The H I extends up to 70 arcsec (1.8 kpc) on both sides of the plane at column densities $N_{\mathrm{H\,I}} = 4.0 \times 10^{19}$ cm^{-2} (3σ). This extent is much more than the FWHM of the beam (26 arcsec) which is clearly seen in Fig. 3. This figure shows the vertical distribution of the data (black solid line) and a Gaussian (blue dot–dashed line) with an FWHM of 26 arcsec. Both are normalized to the maximum of the data. In this figure it is easily observed that the wings of the data are much more extended than the observational beam.

3.2 Velocity distribution

3.2.1 Hα velocities

Fig. 4 shows the velocity field of the PPAK observations. This velocity field was obtained by taking the peak position of the Gaussian fitted to each bin (see Section 3.1.1). This is by no means equal to the actual deprojected maximum rotational velocity in the galaxy but it is an apparent mean velocity determined by a combination of the rotational velocity, the density distribution of the ionized gas, and the opacity of the dust. From here on whenever we mention velocity we are referring to this mean velocity unless otherwise noted. The Gaussian fitting procedure, and therefore the mean velocity, was chosen because with a channel separation of 70 km s^{-1} it is impossible to confidently fit the intrinsic shape of the emission line.

Fig. 5 (left) shows a cut 10-arcsec wide of the velocity field along the major axis. Overplotted are the velocities obtained by Kuzio de Naray et al. (2006) with the DensePAK IFU (blue symbols) and the rotation curve obtained from the modelling (see Section 4). Kuzio de Naray et al. (2006) were not able to trace emission as far out in radius with their observations. Since their exposure time and fibre size is equal to ours this is most likely caused by the fact that they do not bin the data and the lower sensitivity of the DensePak IFU. The velocities obtained by Kuzio de Naray et al. (2006) agree well with our values, which assures us that there are no systematic errors in our reduction or the Gaussian fitting procedure.

In this plot we see clearly that the part of the galaxy observed in our Hα field of view is still resembling a slow rising rotation curve that indicates solid body rotation. This behaviour of the rotation

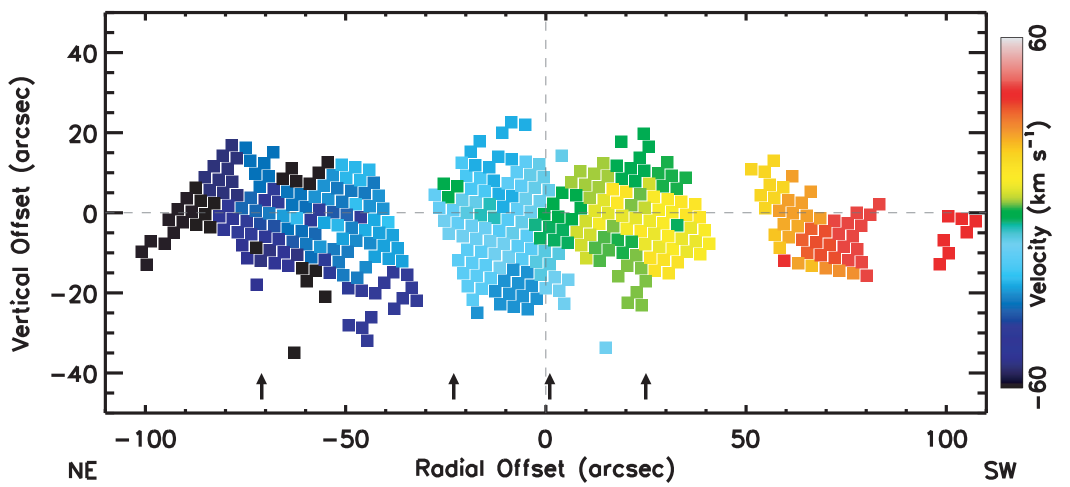

Figure 4. Velocity field of the ionized gas. The field was constructed by taking the central position of the fitted Gaussian in all the binned spectra. The systemic velocity ($V_{\mathrm{sys}} = 156$ km s^{-1}) has been set to 0. The separate pixels show the fibre positions and the colours run from −60 to 60 km s^{-1}. The arrows indicate the positions of the velocity cuts parallel to the minor axis in Fig. 6.

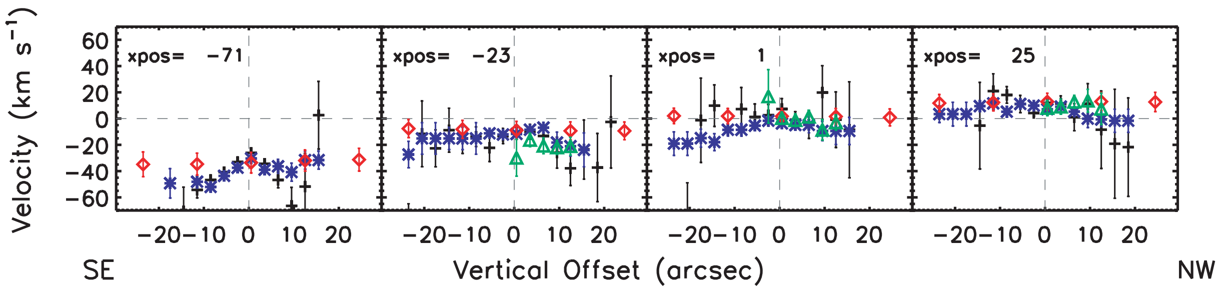

Figure 6. Four cuts parallel to the minor axis through the velocity field at −71, −23, 1, 25 arcsec radial offset from the centre. The negative (positive) offsets are the south-east (north-west) in the sky. Black points are the unbinned PPAK data. Blue, Voronoi binned PPAK data. Red, H I data. Green, Kuzio de Naray et al. (2006) data.

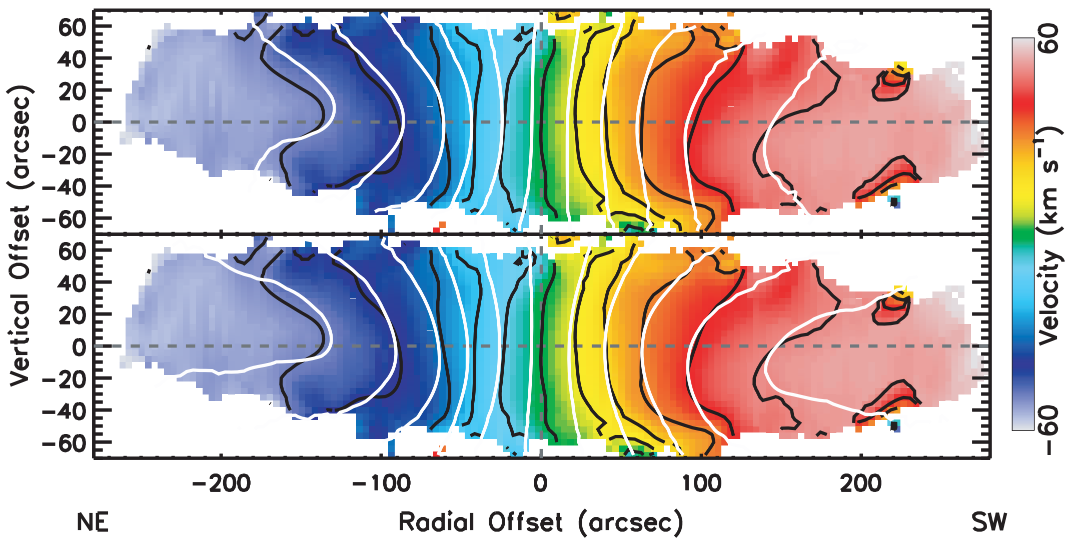

Figure 7. Velocity field of the neutral hydrogen. The field was constructed with the task MOMENTS in GIPSY (see text). Contours are from −60 to 60 km s^{-1} with increasing steps of 10 km s^{-1}. Black contours are the data. The white contours in the upper panel show the line-of-sight warp model. In the lower panel the white contours show the best-fitting edge-on model with a lag of 10.6 km s^{-1} kpc^{-1} (see Section 4).

curve is quite typical of dwarf galaxies, which all seem to have a large inner region in which their rotation curve resembles solid body rotation (Côté, Carignan & Freeman 2000). This slow rise could, in theory, be caused by us considering the mean velocities. However, this is unlikely as we will discuss in Section 3.2.2.

Another thing that is quite clear is that the flux peaks in the Hα along the major axis stand out in the velocity curve as areas with lower velocities (Fig. 5, left, black arrows). This is expected if they are H II regions, since the chance that they would lie on the line of nodes is low, and would imply that most of the peaks we see in the Hα distribution are indeed H II regions. Another possible explanation is that the intensity peaks correspond to a higher density in the radial density profile of the galaxy with thicker clumps offset from the line perpendicular to the line of sight. This explanation is supported by the fact that some of the peaks appear symmetrically around the centre of the galaxy (see Section 3.1.1) and that the star formation rate in UGC 1281 is so low (SFR = 0.0084 M$_\odot$ yr^{-1}) that giant H II regions would not be expected to reside in the galaxy.

If so, this would require that as the influence of the overdensity or H II region, on the shape of the line profile diminishes, the measured velocities should increase. We can see that this is the case when we look away from the mid-plane as is illustrated in Fig. 6. These plots show the velocity as a function of vertical offset from the plane in bins 12-arcsec wide for the binned and unbinned Hα (blue and black, respectively), the data from Kuzio de Naray et al. (2006) (green) and the H I (red) at the positions of the peaks.[2] Here we see that the velocities move away from the systemic velocity as we look higher above the plane. This confirms the idea that the velocities on the major axis are lowered by a line-of-sight projection effect. These results and their implications will be discussed in Section 5.2 in combination with the results of the H I.

3.2.2 *H I velocities*

Fig. 7 shows the velocity field of the H I observations. This velocity field was constructed with the MOMENTS routine in GIPSY by selecting the first moment of the data cube. The routine determines the intensity-weighted mean velocity position of the peak of the line profile in every pixel of the cube. For symmetric profiles, this is analogous to fitting a Gaussian profile to the emission line and taking its velocity at the peak. Since UGC 1281 has only small rotational values, the line profiles are almost symmetric. We have checked this by comparing a map with the velocities where the line profiles have their maximum with this GIPSY map and we find no differences greater than 6 km s^{-1}, which is less than the velocity resolution (see Table 1). Thus, these velocities are in principle comparable one to

[2] Note that also above the major axis, the DensePak data and our data agree within the errors.

one with the velocities of the Hα and differences should be due to the conditions of the gas (distribution effects, dust, resolution, self-absorption or a real difference in the rotational speed of the ionized and neutral gas).

It is common to retrieve the rotation curve of edge-on galaxies through envelope tracing. Theoretically this is the correct way of retrieving the rotation curve of an edge-on galaxy (Sancisi & Allen 1979); however, there are several reasons why Gaussian fitting is preferable in an edge-on dwarf system. As explained in the previous paragraph the velocities in a dwarf galaxy are small, this means that the dispersion of the gas makes up a significant part of the line profile. Since in envelope tracing, either by fitting Gaussians or a scaling of the maximum intensity (Sofue & Rubin 2001), this dispersion is a chosen parameter, it increases the uncertainty of envelope tracing. Furthermore, envelope tracing is also an estimation of the real rotational velocities and detailed modelling is still required. Therefore we prefer the well-understood and well-described method of Gaussian fitting. This does mean that only from the modelling we obtain information about the real rotation curve.

Fig. 5 (right) shows a cut 10 arcsec wide of the velocity field along the major axis. Here we see the same slow rise in the rotation curve as seen in the Hα but we also see that in the H I we do reach the flat part of the rotation curve at ∼120 arcsec radial offset, outside the Hα field of view, from the centre of the galaxy at a maximum velocity ∼60 km s^{-1}.

If we move away from the plane (Figs 7 and 8) we see that the velocities are lower than on the major axis. This implies that either the outer parts of the galaxy are heavily inclined, that the disc is flaring or that the gas above the plane is 'lagging'. We can quantify this vertical velocity gradient in normalized position–velocity (PV) diagrams (see Kamphuis et al. 2007, section 6.2) parallel to the minor axis (Fig. 8, bottom row) by fitting a straight line to the maxima between 20 and 50 arcsec offset from the plane. Of course this fit is affected by the warp, lag, beam smearing and possibly other systematics. Therefore, the measured value has to be compared to the same measurements of models that can explain the observed declining velocities. These models will be presented in the next section and discussed in Section 5.

4 MODELS

The Hα observations show such an irregular distribution that constructing a model for comparison will not bring more insight into the structure of the Hα distribution. Also, the distribution is peaked

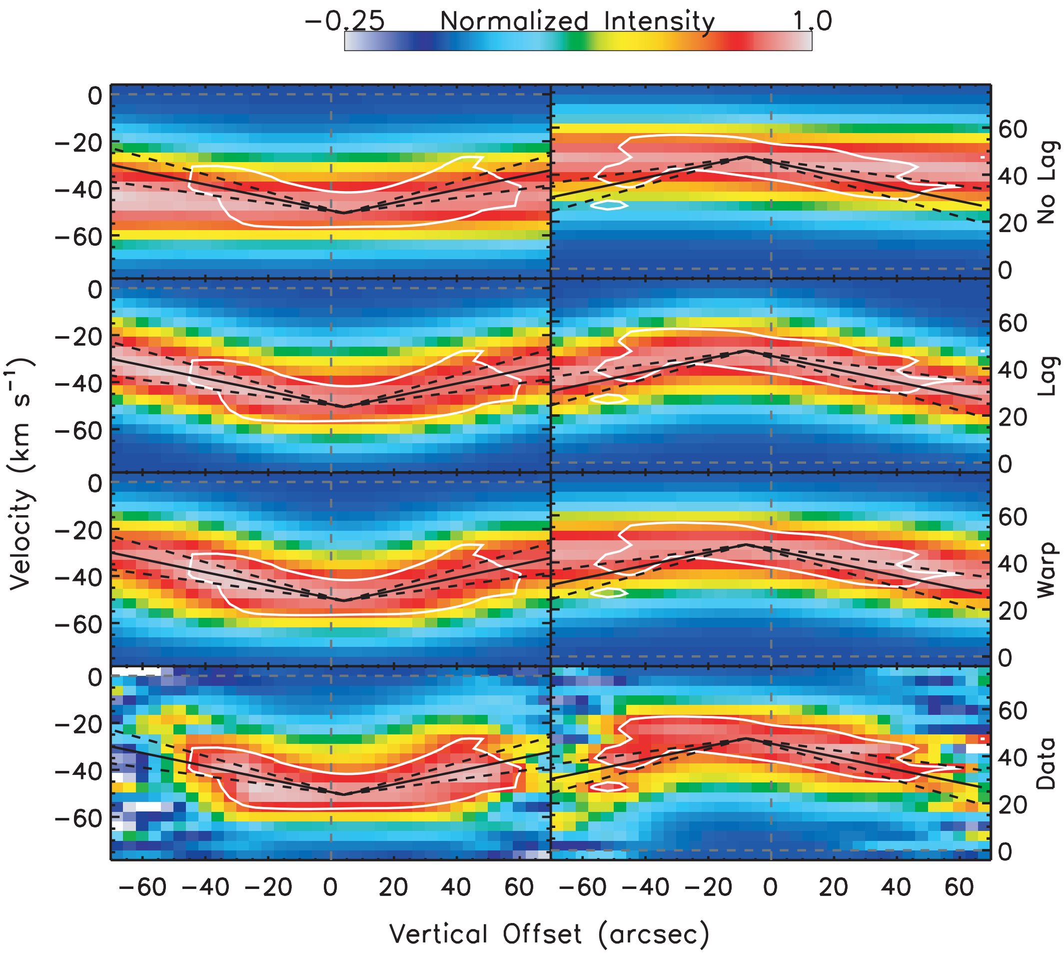

Figure 8. Normalized PV diagrams parallel to the minor axis averaged over 100 arcsec at a radial offset of −175 to −75 arcsec (left) and 75 to 175 arcsec. From top to bottom, the edge-on model without lag, the edge-on model with lag, the line-of-sight warp model and the data. The white contour outlines the 0.75 level of the data. The solid lines show the lag obtained from an edge-on lagging model (see Section 4.1). The dashed lines show the derived error on the lag. The zero-point is set to the point of maximum intensity in a non-normalized PV diagram.

Table 4. Hα parameters that could be measured from the observations or obtained from the literature. References: [1] this paper, [2] van Zee (2001), [3] van Zee (2000).

Parameter	Value	Reference
EM scaleheight	0.22 ± 0.03 kpc	[1]
scalelength	1.09 kpc	[2]
SFR	$0.0084\ M_{\odot}\ yr^{-1}$	[2]
Hα luminosity	$3.81 \pm 0.01 \times 10^{-13}$ erg s^{-1} cm^{-2}	[3]

at many places whereas our models would resemble a smooth exponential distribution. We therefore decided to forego any attempt at modelling the ionized hydrogen in 3D. However, there are several parameters that can be derived from the data or obtained from the literature. These are presented in Table 4 for comparison to the H I model.

4.1 Tilted ring models

To better understand the 3D distribution and the kinematics of the neutral hydrogen in UGC 1281 we have constructed a range of tilted ring models. These models were created with the GIPSY task GALMOD. The GALMOD routine was modified by one of us (GHH) and F. Fraternali to be able to include radial and vertical motions as well as a vertical gradient for the rotational velocities.

The modelling is not straightforward, since many different parameters may be independently fitted and some of them are degenerate. In the case of an edge-on galaxy matters are even more complicated because small changes in density in the outer rings can seriously affect the inner rings of the model. For this reason the fitting always has to start at the outer radii and then move inward ring by ring. Since it is clear that the warp is not symmetric at all, we fit both sides of the galaxy independently. The goodness of a fit was determined by investigating several representations of the data (PV diagrams, residual maps) by eye.

The following, iterative, procedure was followed for the fitting. We start by comparing radial and vertical density profiles of the data with the models (see Fig. 3). This has to be done to get an initial rough estimate of the density profile and scaleheight. When these profiles have a reasonable fit we start fitting the position angle on a integrated moment map. The position angle was deemed to fit when, at all radii, the vertical position of the peak value was equal in the models and the data.

In the tilted ring model the inclination of each ring is related to the position angle and dependent on the angle between the axis on which the ring tilts and the line of sight. We assume a simple warp, where the tilt axies for all rings are aligned, e.g. a straight line of nodes. The assumption of a straight line of nodes is a simplifying one that lowers the degrees of freedom in the model, making it possible to constrain the vertical distribution and kinematics in the model. By assuming a simple warp the inclination of each ring is coupled to its position angle by just one parameter, the angle between the line of sight and the line of nodes. We shall refer to this angle as the warp axis angle.

From the data it is impossible to determine an exact warp axis angle. We therefore set out to find the maximum and minimum warp axis angle that can fit the observations. Starting at a minimum warp axis angle of 0°, e.g. all rings 90° inclined, we found an acceptable density distribution immediately.

We then set out to find the maximum warp axis angle. This maximum is set at the point where the vertical profile starts to show a break, which is not observed in the data (see Fig. 3). By slowly increasing the warp axis angle and comparing the vertical distribution of the model to the data, we find that this break becomes significant when the warp axis angle is greater than 60°, thus defining the maximum line-of-sight warp model to have a warp axis angle less than 60°.

At this stage we split our modelling into two parts. Besides a model with a warp axis angle of 0°, the edge-on model, we construct a second model with a warp axis angle of 55°, the maximum line-of-sight warp model. Now the only parameter of the density that is not determined yet is the vertical distribution of each ring. In our models the vertical density, of all the rings, declines as an exponential of which the steepness is set by its scaleheight. By increasing/decreasing the scaleheight of our models systematically we find the upper and lower limit of the scaleheight. We allow the scaleheight to change from ring to ring but only increase towards larger radii. This increase would resemble a flare. In this way we find that the best-fitting scaleheight of the H I in UGC 1281 is a flaring model that ranges from 10 to 15 arcsec (0.26–0.39 kpc) for our edge-on model and from 7 to 12 arcsec (0.18–0.31 kpc) for our maximum line-of-sight warp model.

In order to estimate the accuracy of our scaleheights we systematically raise and lower the best-fitting flaring model. It turns out that the vertical profile significantly deviates from the observations when we add (subtract) more than 4 arcsec (2 arcsec) (100 and 50 pc, respectively) to the scaleheights of our best-fitting models. The vertical distributions of these models are shown in Fig. 3 as blue triangles (upper limit) and red diamonds (lower limit) for the edge-on model. The blue dot–dashed line indicates the spatial resolution (FWHM = 26 arcsec).

As a last check on the density distribution we construct an integrated moment map of the residual cube. Fig. 9 shows the residual map of the best-fitting density distribution. This figure shows only the density distribution of the best-fitting edge-on model because, above the sensitivity limit of the data, the differences in the density distribution between the two models are less than 5 per cent. Therefore the difference between these two models would not be visible in such plots. In this figure the wiggles that necessitate adding a warp, purely in PA, to the edge-on model, and their reproduction in this model, are clearly seen.

After we obtain a satisfactory density distribution, we start fitting the rotation curve and dispersion of the gas. Initially we set the dispersion of the gas to be constant at 9 km s^{-1} and then start fitting the rotation curve. As a first guess for a lower limit of the rotation curve we use the velocities from the Hα and H I. For the inner ±50 arcsec we use the Hα velocities and beyond this point we use the velocities obtained from the H I first moment map (see Fig. 5). This rotation curve is then raised from the outside in until it fits the data.

As an upper limit we start from a flat rotation curve and fit this curve by lowering the velocities from the inside out. The change between rings is always the half of the difference between the previous two rings, with a minimal increase of 4 km s^{-1} for the inner rings. Because a low inner density could artificially lower the observed velocities in an edge-on system, we have set the densities of the inner rings to zero while fitting this rotation curve.

Once more the fitting is an iterative process where the goodness of fit is determined by comparing the major axis PV diagram of the data to the model. An example of such a PV diagram is shown in Fig. 10, where the best-fitting edge-on model is plotted with the data. The colour scheme and the black contours are the data whereas the red contours display our best-fitting edge-on

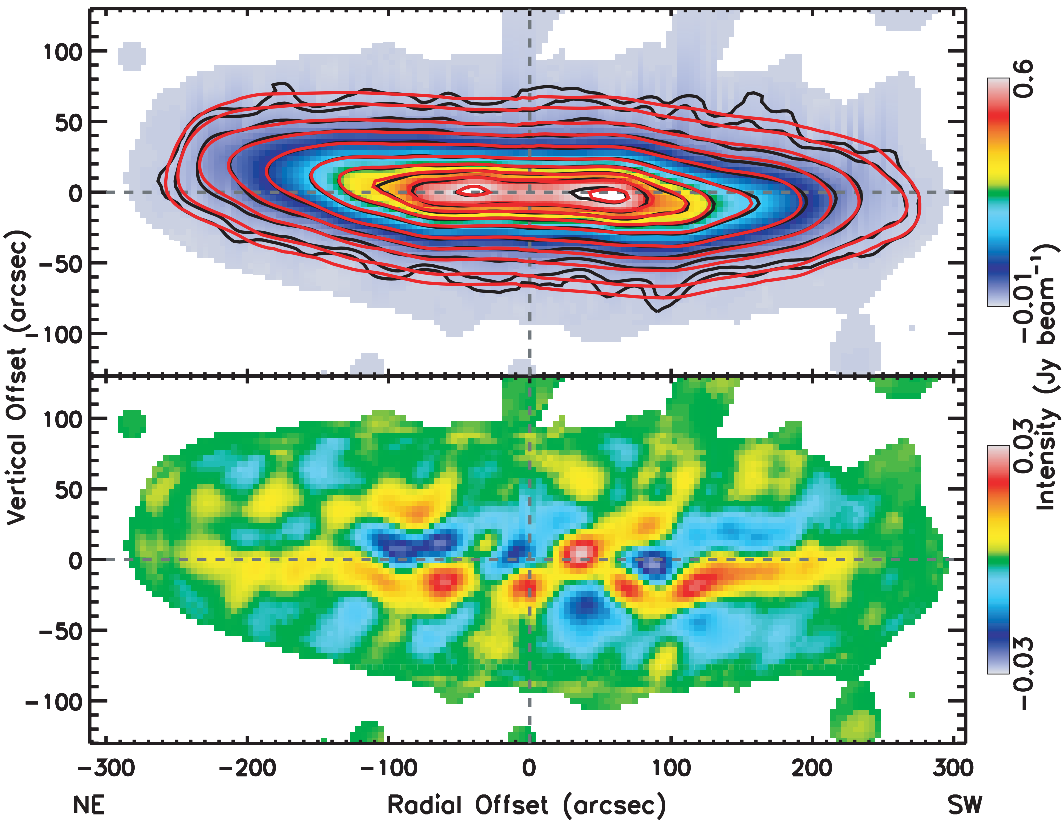

Figure 9. Upper panel: integrated H I flux map of UGC 1281 (see Fig. 2). The black contours are the data at the same levels as in Fig. 1. The red contours are the same levels for the best-fitting edge-on model. Lower panel: residual map of the data minus the best-fitting edge-on model (total intensity).

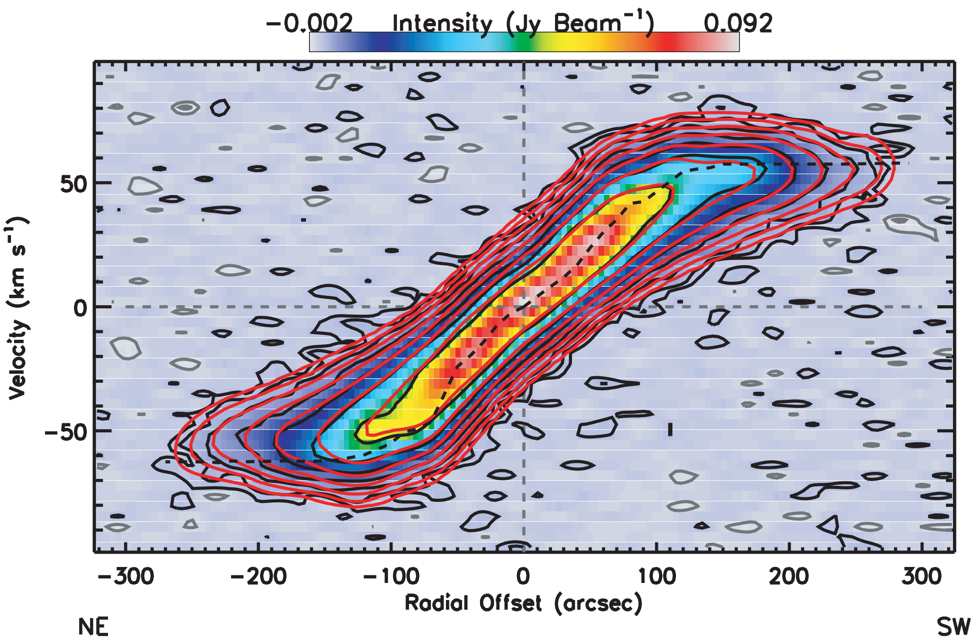

Figure 10. Colour plot of the H I PV diagram along the major axis. Overlaid with contours of the data (grey/black) and the best-fitting model (red). The contour levels are -3σ, -1.5σ, 1.5σ, 3σ and 6σ ($1\sigma = 0.5$ mJy beam^{-1}) etc.

model. Again only the edge-on model is shown because also in this PV diagram the differences between the two models are less than 5 per cent. When we have obtained satisfactory fits to this PV diagram for both the upper and lower limit rotation curves, we find that they differ no more than a channelwidth (4.1 km s^{-1}) at any ring position, which indicates that the rotation curve is well constrained. Besides the upper- and lower-limit rotation curves matching very well, also the rotation curves of both, independently fitted, sides of the galaxy match up quite well. The final rotation curves are shown in Figs 5 and 14 (top panel). These curves are the average of the upper and lower limit of both the best-fitting models. Fig. 10 shows the rotation curve of the best-fitting edge-on model as a black dashed line overlaid on the major axis PV diagram.

After fitting the rotation curve we found that the fit to the major axis PV diagram could be significantly improved by introducing a gradient in the velocity dispersion. This gradient runs from $\sigma_v = 11\,\mathrm{km\,s^{-1}}$ in the centre to $\sigma_v = 8\,\mathrm{km\,s^{-1}}$ at the largest radii (see Fig. 14, bottom panel).

The model cubes should now be comparable to the data cube everywhere and any major deviations can only be caused by gas that is deviating from corotation at high projected distances from the mid-plane. In the case of the maximum line-of-sight warp model the observations are fully reproduced by the best-fitting model. However, in the case of the edge-on model the velocities above the plane are clearly over estimated. This can be seen in Fig. 8. When we compare the edge-on model (upper panels) to the data (lower panels), it is easily seen that in the data the emission peaks at a vertical offset lie at lower velocities than the emission peak in the mid-plane. However, such a bending is only produced by the warp when the rings are not edge-on and thus completely lacking in the edge-on model without a lag. Therefore, we reproduce the edge-on model with a rotation curve that declines as a function of the distance to the plane, e.g. a lag. We construct seven models where the vertical gradient is increased from 4 to 28 $\mathrm{km\,s^{-1}\,kpc^{-1}}$ in steps of 4 $\mathrm{km\,s^{-1}\,kpc^{-1}}$.

When we measure the vertical gradient in these models in the same way as in the data (see Section 3.2.2), we find that the value measured from the data corresponds to a lag of $10.6 \pm 3.7\,\mathrm{km\,s^{-1}\,kpc^{-1}}$ (see Fig. 11) in the edge-on model. After adding this lag to the model it was found that, due to beam smearing effects, the major axis PV diagram showed emission at slightly lower velocities than the data and the line-of-sight warp model. To correct for this effect the flat part of the input rotation curve was raised by $2\,\mathrm{km\,s^{-1}}$. With this correction the major axis PV diagrams of both models agreed within 5 per cent again. A model with this lag produces a satisfactory fit at all heights.

As a last check on the model we compare the non-lagging model to the data and the lagging edge-on model in PV diagrams at two distances above (below) the mid-plane. Figs 12 and 13 show PV diagrams parallel to the major axis at ±26 and ±56 arcsec offset from the plane. Already Fig. 12 is suggesting that a model with a lag gives a better fit, though we cannot exclude the non-lagging model at this height. At a height ∼60 arcsec above the plane (Fig. 13), it is clearly seen that the velocities around the 3σ contours are too high in the non-lagging model.

Fig. 8 shows also the normalized PV diagrams parallel to the minor axis for the best-fitting lagging edge-on model. Also in these figures it is now seen that the edge-on model with a vertical gradient and the maximum line-of-sight warp model fit the data equally well.

Fig. 14 shows the parameters for the best-fitting models of UGC 1281 [edge-on model (black lines) and line-of-sight warp model (symbols)]. The best fit for the edge-on model has a flare and the scaleheight ranges from 10 arcsec (0.26 kpc) in the inner parts to a maximum of 15 arcsec (0.39 kpc) on the north-eastern outer parts. The change in PA is the same for both models but in the case of the line-of-sight warp model, this is coupled to a change in inclination of the ring as previously explained. The scalelength of this model galaxy is 46 arcsec (1.2 kpc). The scalelength is the same for the maximum warp model, which is also flaring and has a scaleheight of 7 arcsec (0.18 kpc) in the inner parts and 12 arcsec (0.31 kpc) in its outer parts.

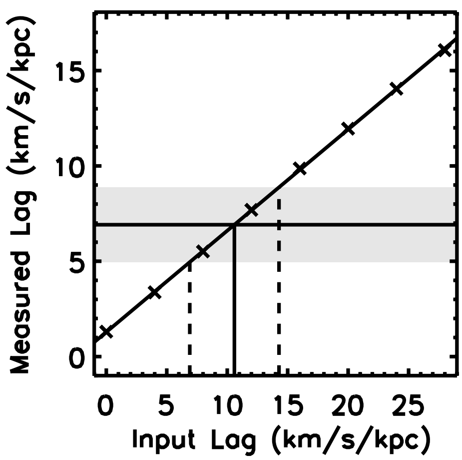

Figure 11. Input lag versus Measured lag in the models. The solid line shows the fit to the measured values (displayed by crosses) of the models. The horizontal solid line displays the value obtained from the data. The vertical solid line shows where the measured value intersects the model fit. The grey shaded area indicates the error in the measurement and the dashed vertical lines where the error intersects the fit. This range determines the error bar on the value of the lag.

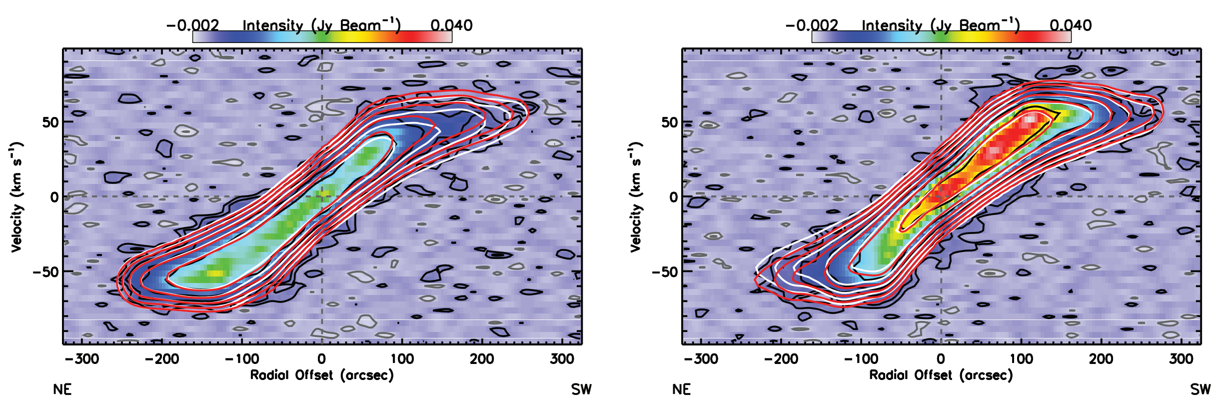

Figure 12. Left (right): Colour plot of the H I PV diagram at 26 arcsec (−26 arcsec) (±0.6 kpc) offset from the major axis. Contours are at −3σ, − 1.5σ, 1.5σ, 3σ, 6σ and so on. The black solid contour is the data, the red contour is the best-fitting model with no lag and the white contour is the best-fitting model with an assumed vertical gradient of 10.6 $\mathrm{km\,s^{-1}\,kpc^{-1}}$ in the rotation curve. The colour map ranges are indicated above the panel in Jy beam^{-1}.

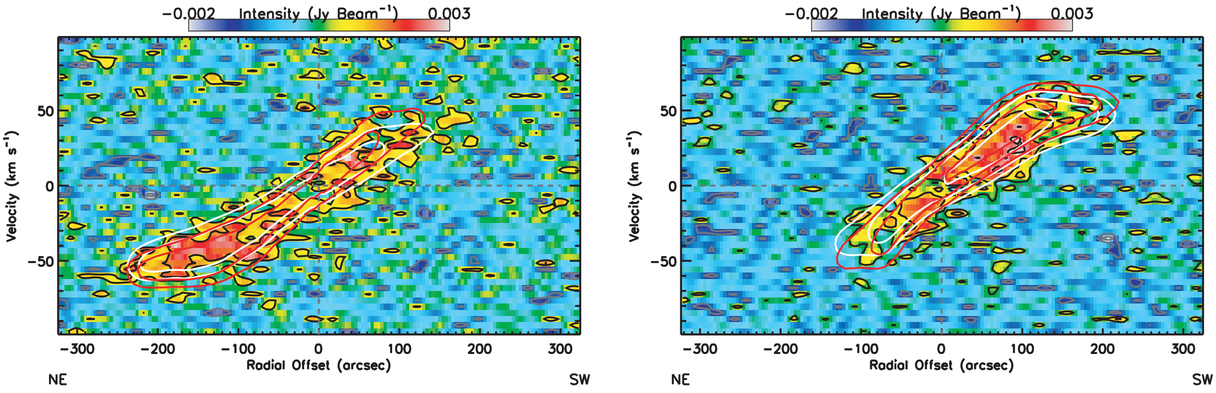

Figure 13. Same as Fig. 12 but now at ±56 arcsec (±1.3 kpc) offset from the plane.

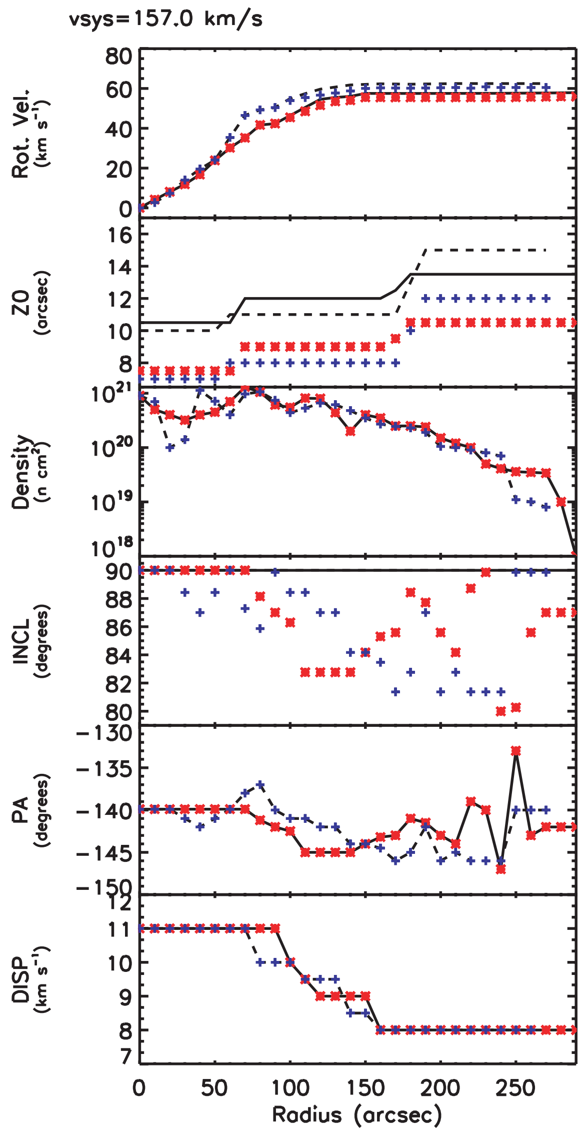

Figure 14. Model parameters as a function of radius. For the edge-on model (solid line, south-west side; dashed line, north-east side) and the maximum line-of-sight warp model (blue pluses, south-west side; red crosses, north-east side).

4.2 Ballistic models

To investigate what we would expect for UGC 1281 in the sense of extraplanar gas brought up from the disc by supernovae, we have used the ballistic model of Collins, Benjamin & Rand (2002). In this model gas is blown out of the disc into the halo, with an initial vertical velocity (called the kick velocity). The model naturally predicts a vertical gradient in rotational velocity which has a higher magnitude in model with a high kick velocity. To obtain the vertical gradient of the model we follow the procedure outlined by Heald et al. (2007), with the following difference. The initial disc for the model is infinitely thin; this is because the scaleheight of the Hα in UGC 1281 is already comparable to the scaleheight normally used for the initial disc (0.2 kpc). Therefore this model should be thought of as an absolute upper limit on the kick velocity.

We find that the scaleheight of 0.2 kpc is reproduced when the initial kick velocity is 10 km s^{-1}. We run the simulation until the system reaches steady state (∼1 Gyr). At this point there are no clouds in the halo at radii smaller than 4 kpc due to the radial outward movement of the clouds. Therefore we cannot measure the vertical gradient in the rotational speed at these radii. However, at radii between 5 and 10 kpc we find a small gradient of 0.4 km s^{-1} kpc^{-1}. This is a very low value as one would expect of a small galaxy like UGC 1281 since kick velocities must be small at a low potential, because otherwise the scaleheight becomes too large.

5 DISCUSSION

5.1 Hydrogen in the plane

When we compare the parameters of the best-fitting H I models to the parameters extracted from the Hα data (Table 4) we see that compared to the ionized gas the neutral gas is much more extended in the radial direction. Apart from this its scalelength is slightly larger. So, the ionized gas is more centrally concentrated than the H I.

Note that both the neutral gas and the ionized gas display a central depression, or peaks symmetrically around the centre, in their distribution (see Section 3.1). Also, the Hα distribution is more irregular than the neutral hydrogen. This can easily be seen in Figs 1 and 2 by counting peaks in the distribution (see Section 3.1.1). One of these 'peaks' in Hα has a clear offset from the plane of the galaxy and this region does not stand out in the H I observations.

Another effect is the start of the warp. If we look at the integrated moment maps the neutral gas starts to deviate from the major axis at a radius almost two times larger than the radius where the

Hα bends away from the major axis (50 and 90 arcsec, respectively). Most likely this is a resolution effect, because when we look at the best-fitting model for the H I we see both the H I and the Hα start to warp around 50 arcsec (1.3 kpc).

When we compare the measured velocities of the neutral and ionized gas they look very similar on the major axis (see Fig. 5). Ideally this should only occur if the sizes of both discs are similar and there is no absorption, self-shielding or clumpiness affecting the emission. We know from the analysis of the Hα that the velocities in the plane are lower than those above the plane in several places. Also, the H I velocities are slightly lower, due to beam smearing, when compared to the best-fitting model. Since for the Hα emission we can only look at the rising part of the rotation curve, where the rotational velocities are low, deviations from the real rotational velocities are small. Therefore, it is not unreasonable that both effects provide us with the same velocities since all the absolute deviations from the rotational velocities are small. Fig. 5 (red line) shows that the real rotation curve, obtained from the modelling, is slowly rising and reaches a flat part around 60 km s^{-1}. This means that UGC 1281 has a slow rising rotation curve which is common in dwarf galaxies, but it also shows a clear differential rotation.

5.2 Hydrogen above the plane

We see (Fig. 1) that the Hα extends less far in the vertical direction than the H I. Despite the fact that a difference in sensitivity may cause us to miss Hα emission at distances farther from the plane than 20 arcsec, the scaleheight, measured by fitting a single exponential to the vertical distribution, of the Hα is, equal at best, but most likely smaller than the H I scaleheight.

Even though the vertical extent of the Hα is limited and not supplying much information above the plane, the H I extends well above the plane and much can be learned from it. If we assume a constant gas dispersion of 9 km s^{-1}, we would expect a scaleheight of ∼400 pc for the disc, from a simple estimate (Puche et al. 1992). This implies that the gas at large distances from the mid-plane is not an additional component but merely the high-latitude gas of a pressure-supported disc. This idea is strengthened by the fact that a ballistic model requires a very low kick-velocity (∼10 km s^{-1}), of the order of the velocity dispersion in the model, and indicates that the gas at large distances from the mid-plane is not pushed to high latitude by star formation processes. Furthermore, continuum maps constructed from the line-free channels of the 21-cm observations do not show any continuum emission at the position of UGC 1281, once more confirming the low SFR. This implies that UGC 1281 does not contain a typical halo such as that seen in NGC 891. However, also in the case of UGC 1281 the kinematics show that as the distance from the mid-plane increases, the projected mean velocities decline (see Fig. 8).

From our modelling we obtain two possible explanations for the high-latitude H I and its declining projected mean velocities. We find that a maximum line-of-sight warp model, where we push the warp as much into the line of sight as the data allow, fits the data equally well as a purely edge-on model with a warp in the plane of the sky and a vertical gradient in its rotation curve of -10.6 ± 3.7 km s^{-1} kpc^{-1}. Both models assume a single exponential in the vertical direction and the edge-on model does assume that the radial gas distribution above the plane is similar to that in the disc. In theory the lower velocities could also be caused by an alternative distribution above the disc. However, since the vertical gradient is seen almost everywhere in the observations, it seems unlikely that this is the case unless the gas is in a warp or flare and these possibilities are included in the modelling.

To outline the importance of separating between a lag and a line-of-sight warp we will discuss these two options and their implications in two separate sections below. These discussions are by no means meant to be a complete overview of the theory and observations behind extraplanar gas but only to highlight the parts where UGC 1281 can significantly contribute to a better understanding of the theories. For a full and complete review of cold extraplanar gas we refer the reader to Sancisi et al. (2008) and references therein.

5.2.1 A warp

The first possibility that can explain the observations is that the gas at large projected distances from the mid-plane in UGC 1281 is located in a simple warp. Warps are quite common in disc galaxies and often they are asymmetric (García-Ruiz et al. 2002) as is observed in UGC 1281. If the H I and its kinematics in UGC 1281 are to be fully explained by a warp, the warping axis has to have an angle of 55° with respect to the line of sight.

We would like to point out the very small differences between the edge-on model and the maximum line-of-sight warp model. The maximum difference in inclination between the two models is 10° but on average 5° in inclination. This results in a difference in scaleheight of ∼3 arcsec (see Fig. 14). These differences take away the need for a vertical gradient completely. This once more shows that differences between line-of-sight warps and lagging haloes are very subtle, and that great care must be taken to exclude one of the two options.

When we measure once more the maxima in normalized PV diagrams parallel to the minor axis, we find an apparent vertical gradient of 4.9 ± 1.1 km s^{-1} kpc^{-1}, for the maximum line-of-sight warp model, which is consistent with the measurement from the data (6.9 ± 2.0 km s^{-1} kpc^{-1}). Therefore, there is no need to introduce a lag or other extra kinematical effects into this model.

The best-fitting model for this case has central scaleheights which are similar to those measured from the stars and the Hα. This would mean that the stars and the ionized gas hardly extend into the warped outer regions of the disc and that all the H I at large projected distances from the mid-plane is in the warp and flare. We have already seen that the PA starts changing well within the maximum radius of the Hα as well as inside the optical radius. This is seen for every model, whether it is edge-on or maximum line of sight.

The start of the warp could be affected by a slight error in the assumed PA. We have tested this by rotating the integrated H I moment map and the red DSS image (see Fig. 2) by an additional 1° and 2° (PA = 39° and 38°, respectively) and plotting the vertical offsets of the peak of the vertical profiles. This shows that for the red optical image the PA of 40° gives the flattest central distribution but that the start of the warp in the H I can be pushed outward by ∼15 arcsec by assuming a PA of 39°. This means that the observed start of the warp remains well within the optical radius ($\frac{1}{2}D_{25} =$ 134 arcsec) even if the assumed PA is slightly off.

The fact that the warp starts within the optical radius is inconsistent with the findings of van der Kruit (2007) that warps start just beyond the truncation radius of the stellar disc. Even more so, we know from the observed Hα emission that also the ionized gas is slightly warped (see Section 3.1.1). This would imply that if the warp in UGC 1281 is formed by the accretion of gas from the IGM its initial disc was not rigid enough to stabilize the infalling gas (van der Kruit 2007). If so, one would expect a clear difference between the onset of the warp, with respect to its truncation radius, between dwarf galaxies and massive galaxies.

5.2.2 *A lag*

In the case of a warp which is purely in the plane of the sky, the modelling indicates a larger scaleheight of the H I than the scaleheights measured from the stars and the ionized hydrogen. This vertical density distribution can be modelled with a single exponential; however, the kinematics indicate the need for a vertical gradient in the rotation curve when the warp is purely perpendicular to the line of sight. As in the case of the superthin galaxy UGC 7321 (Matthews & Wood 2003), the origin of this lagging neutral hydrogen gas in an LSB dwarf galaxy, with low star formation rates, would be puzzling.

If the high-latitude gas in UGC 1281 is lagging this would have some implications for the current theory. Heald et al. (2007) have compared the lag, or the vertical gradient in the rotation curve in three massive galaxies. They have found tentative evidence that when they scale the lag with the observed Hα scaleheight[3] this new parameter ($\mathrm{d}V/\mathrm{d}h_z$) is roughly constant at about 20 km s^{-1} scaleheight^{-1}. However, the galaxies compared are of similar mass. The results presented in this paper give us now the opportunity to take a tentative look at a class of galaxies with much lower mass. The dynamical mass of UGC 1281 is $6.3 \times 10^9\,\mathrm{M}_\odot$, measured at our last point of the rotation curve, as opposed to $\sim 1 \times 10^{11}\,\mathrm{M}_\odot$ for the galaxies in the study by Heald et al. (2007).

Within the picture of a lagging disc, we would have $\mathrm{d}V/\mathrm{d}h_z = 4.7 \pm 1.7$ km s^{-1} per scaleheight. This value would be inconsistent with a constant $\mathrm{d}V/\mathrm{d}h_z \sim 20$ km s^{-1} which was found for the three massive galaxies. As shown by the ballistic models (Section 4.2), the lag expected purely on gravitational grounds would be much shallower than the one that we include in this model. Such a lag would thus require an additional effect to be at play such as those described by e.g. Benjamin (2002); Barnabè et al. (2006); Fraternali & Binney (2008). In any case, star formation in the disc would be of negligible influence on the vertical gradient.

The above discussion clearly shows the need to unambiguously determine a lag in a small galaxy such as UGC 1281 as well as the need for a larger sample of galaxies with quantified vertical velocity gradients. In the present case, due to the fact that the addition of a lag to the model of UGC 1281 does not significantly improve the match with the data, we prefer the conceptually simpler line-of-sight warp model.

6 SUMMARY

We have presented 21 cm and Hα emission in the edge-on dwarf galaxy UGC 1281. This is the first time such sensitive H I data have been presented for a dwarf edge-on.

The integrated Hα velocity map (Fig. 1) shows a non-smooth distribution on the major axis with several peaks. One of these peaks is actually located beneath the major axis. It is unclear whether this H II region is located above the plane of the galaxy or in its warped outer parts.

The integrated H I velocity map (Fig. 2) shows a quite regular distribution with a central depression. This central depression appears to be symmetrical in position around the centre but from modelling it follows that it is somewhat deeper on the NE side of the galaxy. Such a central depression is not uncommon for dwarf galaxies.

Furthermore this map shows that UGC 1281 is warped in its outer parts and this warp resembles a ‘normal’ S-shape at its start. However, at large radii the warp bends back towards the inner plane of the galaxy.

For the interpretation of the kinematics of the high-latitude H I gas, we have constructed velocity maps from the Hα and H I data. Also, 3D models with a modified version of GALMOD are constructed in GIPSY. This modified version enables us to construct kinematic models with a vertical gradient.

The velocities obtained from the data show a slow rise in the inner part. This is also seen in the rotation curve obtained from the modelling and therefore unlikely to be an effect of the H I distribution or resolution. At about 120 arcsec the rotation curve flattens off to a maximum rotational velocity $\sim$60 km s^{-1}. This slow rise is common for dwarf galaxies.

From our modelling we find that our data are not sensitive enough to distinguish between a lag or a line-of-sight warp. Both models fit the data equally well and there is only a small difference between the input parameters of the models. However, the models do start to deviate at emission levels slightly lower than our current sensitivity limit. Therefore, one would most likely be able to separate between the two models with deeper observations.

In the case of lagging high-latitude gas the low vertical extent and the low flux level of the Hα emission indicate that this high-latitude H I does not originate from galactic fountains. The H I scaleheight implies a normal pressure supported disc and thus no need beyond turbulence for a mechanism to bring it up from the mid-plane. If in such a disc the pressure, of the gas, is solely dependent on the density (e.g. barytropic), one would expect it to be corotating. However, we find in our analysis that the high-latitude gas in this case has a lag of 10.6 ± 3.7 km s^{-1} kpc^{-1} when compared to tilted ring models. This lag could be caused by infalling gas or pressure gradients above the mid-plane.

In the case of a line-of-sight warp the ionized hydrogen and the distribution of the stars would, for the most part, not extend into the warped region of the disc. However, the scaleheight in the central parts would be the same for the stars, Hα and H I.

Regardless of which model fits the data best, maximum line-of-sight warp or edge-on, the warp starts well with the optical radius [$D_{25} = 4.46$ arcmin, de Vaucouleurs et al. (1992)], at a radius of $\sim$50 arcsec, which is unlike more massive galaxies (van der Kruit 2007).

The small differences in input parameters between a model with a lag and one with a line-of-sight warp show that great care must be taken to distinguish between lagging haloes and line-of-sight warps since small changes in the modelling can have a great effect on the velocity field.

Our main conclusions can be summarized as follows.

(i) The rotation curve of UGC 1281 slowly rises in its inner parts and flattens off to a maximum rotational velocity $\sim$60 km s^{-1} at 120 arcsec (3.14 kpc).

(ii) The neutral hydrogen in UGC 1281 is more extended than the stars and the ionized emission in its radial distribution.

(iii) The gaseous warp starts well within the optical radius.

(iv) Our observations can be fitted by both a vertical gradient in the rotation curve and a line-of-sight warp. The observations are not sensitive enough to separate between these two options. However,

[3] Note that Heald et al. (2007) use electron scaleheights instead of the emission measure scaleheights.

the line-of-sight warp model is conceptually simpler and therefore preferable.

ACKNOWLEDGMENTS

We thank R. Kuzio de Naray for making her velocity data available to us. We are grateful to S. Sanchez and A. Guijarro for doing the PPAK observations and M. Verheijen for introducing us to PPAK. Many thanks to T. Oosterloo for help with the H I data reduction and to P. Serra, R.-J. Dettmar, D. J Bomans and our anonymous referees for useful comments, discussion and insights.

REFERENCES

Barbieri C. V., Fraternali F., Oosterloo T., Bertin G., Boomsma R., Sancisi R., 2005, A&A, 439, 947
Barnabè M., Ciotti L., Fraternali F., Sancisi R., 2006, A&A, 446, 61
Benjamin R. A., 2002, in Taylor A. R., Landecker T. L., Willis A. G., eds, ASP Conf. Ser. Vol. 276, Seeing Through the Dust: The Detection of HI and the Exploration of the ISM in Galaxies. Astron. Soc. Pac., San Francisco, p. 201
Bomans D. J., Weis K., 2008, in de Koter A., Smith L. J., Waters L. B. F. M., eds, ASP Conf. Ser. Vol. 388, Mass Loss from Stars and the Evolution of Stellar Clusters. Astron. Soc. Pac., San Francisco, p. 395
Boomsma R., Oosterloo T. A., Fraternali F., van der Hulst J. M., Sancisi R., 2008, A&A, 490, 555
Bregman J. N., 1980, ApJ, 236, 577
Cappellari M., Copin Y., 2003, MNRAS, 342, 345
Collins J. A., Benjamin R. A., Rand R. J., 2002, ApJ, 578, 98
Côté S., Carignan C., Freeman K. C., 2000, AJ, 120, 3027
de Vaucouleurs G., de Vaucouleurs A., Corwin H. G., Jr, Buta R. J., Paturel G., Fouque P., 1992, VizieR Online Data Catalog, 7137, 0
de Zeeuw P. T. et al., 2002, MNRAS, 329, 513
Fraternali F., Binney J. J., 2008, MNRAS, 386, 935
Fraternali F., Oosterloo T. A., Sancisi R., Swaters R., 2005, in Braun R., ed., ASP Conf. Ser. Vol. 331, Extra-planar Gas. Astron. Soc. Pac., San Francisco, p. 239
García-Ruiz I., Sancisi R., Kuijken K., 2002, A&A, 394, 769
Heald G. H., Rand R. J., Benjamin R. A., Bershady M. A., 2006, ApJ, 647, 1018
Heald G. H., Rand R. J., Benjamin R. A., Bershady M. A., 2007, ApJ, 663, 933
Hoeft M., Gottlöber S., 2010, Adv. Astron., 2010, 693968
Hummel E., Beck R., Dettmar R.-J., 1991, A&AS, 87, 309
Kamphuis P., Peletier R. F., Dettmar R.-J., van der Hulst J. M., van der Kruit P. C., Allen R. J., 2007, A&A, 468, 951
Karachentsev I. D., Karachentseva V. E., Huchtmeier W. K., Makarov D. I., 2004, AJ, 127, 2031
Kelz A. et al., 2006, PASP, 118, 129
Kuzio de Naray R., McGaugh S. S., de Blok W. J. G., Bosma A., 2006, ApJS, 165, 461
Lee S.-W., Irwin J. A., Dettmar R.-J., Cunningham C. T., Golla G., Wang Q. D., 2001, A&A, 377, 759
Makarova L. N., Karachentsev I. D., 1998, A&AS, 133, 181
Matthews L. D., Wood K., 2003, ApJ, 593, 721
Oosterloo T., Fraternali F., Sancisi R., 2007, AJ, 134, 1019
Pilyugin L. S., Contini T., Vílchez J. M., 2004, A&A, 423, 427
Puche D., Westpfahl D., Brinks E., Roy J., 1992, AJ, 103, 1841
Rossa J., Dettmar R.-J., 2003, A&A, 406, 505
Sancisi R., Allen R. J., 1979, A&A, 74, 73
Sancisi R., Fraternali F., Oosterloo T., van der Hulst T., 2008, A&AR, 15, 189
Sault R. J., Teuben P. J., Wright M. C. H., 1995, in Shaw R. A., Payne H. E., Hayes J. J. E., eds, ASP Conf. Ser. Vol. 77, Astronomical Data Analysis Software and Systems IV. Astron. Soc. Pac., San Francisco, p. 433
Schaap W. E., Sancisi R., Swaters R. A., 2000, A&A, 356, L49
Shapiro P. R., Field G. B., 1976, ApJ, 205, 762
Sofue Y., Rubin V., 2001, ARA&A, 39, 137
Swaters R. A., Balcells M., 2002, A&A, 390, 863
Swaters R. A., Sancisi R., van der Hulst J. M., 1997, ApJ, 491, 140
Valdes F., 1995, Guide to the HYDRA Reduction Task DOHYDRA
van der Hulst J. M., Terlouw J. P., Begeman K. G., Zwitser W., Roelfsema P. R., 1992, in Worrall D. M., Biemesderfer C., Barnes J., eds, ASP Conf. Ser. Vol. 25, Astronomical Data Analysis Software and Systems I. Astron. Soc. Pac., San Francisco, p. 131
van der Hulst J. M., van Albada T. S., Sancisi R., 2001, in Hibbard J. E., Rupen M., van Gorkom J. H., eds, ASP Conf. Ser. Vol. 240, Gas and Galaxy Evolution. Astron. Soc. Pac., San Francisco, p. 451
van der Kruit P. C., 2007, A&A, 466, 883
van Zee L., 2000, AJ, 119, 2757
van Zee L., 2001, AJ, 121, 2003
Westmeier T., Braun R., Thilker D., 2005, A&A, 436, 101

This paper has been typeset from a TEX/LATEX file prepared by the author.